An Investigation of the Effect of Pore Scale Flow on Average Geochemical Reaction Rates Using Direct Numerical Simulation

Sergi Molins[1]

David Trebotich[2]

Carl I. Steefel[1]

Chaopeng Shen[2]

[1]Earth Sciences Division

Lawrence Berkeley National Laboratory

One Cyclotron Road, Mail Stop 90R1116, Berkeley, California 94720, USA

[2]Computational Research Division

Lawrence Berkeley National Laboratory

One Cyclotron Road, Mail Stop 50A-1148, Berkeley, California 94720, USA

Abstract

The scale-dependence of geochemical reaction rates hinders their use in continuum scale models intended for the interpretation and prediction of chemical fate and transport in subsurface environments such as those considered for geologic sequestration of CO_2. Processes that take place at the pore scale, especially those involving mass transport limitations to reactive surfaces, may contribute to the discrepancy commonly observed between laboratory-determined and continuum-scale or field rates. Here, the dependence of mineral dissolution rates on the pore structure of the porous media is investigated by means of pore scale modeling of flow and multicomponent reactive transport. The pore scale model is comprised of high performance simulation tools and algorithms for incompressible flow and conservative transport combined with a general-purpose multicomponent geochemical reaction code. The model performs direct numerical simulation of reactive transport based on an operator-splitting approach to coupling transport and reactions. The approach is validated with a Poiseuille flow single-pore experiment and verified with an equivalent 1D continuum-scale model of a capillary tube packed with calcite spheres. Using the case of calcite dissolution as an example, the high resolution model is used to demonstrate that non-uniformity in the flow field at the pore scale has the effect of decreasing the overall reactivity of the system, even when systems with identical reactive surface area are considered. The effect becomes more pronounced as the heterogeneity of the reactive grain packing increases, particularly where the flow slows sufficiently such that the solution approaches equilibrium locally and the average rate becomes transport-limited.

1. Introduction

Geologic sequestration of CO_2 is considered one of the viable approaches for mitigating the climatic impact of greenhouse gas emissions [White el al., 2003, Pacala and Socolow, 2004]. However, knowledge of the fate of CO_2 injected into deep subsurface aquifers, particularly over long time periods (thousands of years), is still inadequate [Bruant et al., 2002]. Similar limitations exist for other subsurface environments where the interpretation and prediction of chemical fate and transport is essential. These include contaminated subsurface systems [e.g. Bain et al., 2001; Essaid et al, 2003; Steefel et al., 2003; Prommer et al., 2006; Molins et al., 2010], chemical weathering [e.g., Maher et al, 2009], and redox stratified biogeochemical systems [e.g., Wang et al, 2003; Thullner et al, 2005; Li et al, 2009]. Geochemical transport modeling has served as a valuable predictive tool in evaluating sequestration scenarios, but there are limitations to the application of continuum reactive transport models to such systems [Steefel et al., 2005]. Traditionally, the consideration of flow and reactive transport in subsurface porous media has focused on treating the media as continuous domains with macroscopic flow and transport parameters such as hydraulic conductivity, porosity, dispersivity, as well as geochemical parameters such as reactive surface area and reaction rates. In these formulations, flow is usually assumed to obey phenomenological laws, e.g., Darcy's law [Zhang et al., 2000]. Similarly, reactive surface area is estimated from adsorption isotherms (Brunauer-Emmett-Teller, or BET) or geometrically based on the average physical grain size, but this approach does not account for the hydrologic accessibility of the reactive phases within the pore structure [Maher et al, 2006; Peters, 2009]. The

problem is perhaps particularly acute for geochemical processes, since geochemical parameters are often determined for pure mineral suspensions that do not account for the pore structure of the media. It has been long realized that these parameters are scale-dependent and mass transport limitations can introduce large deviations from volume-averaged processes [Li et al., 2006, L. Li et al., 2008]. The pore-scale variation of species concentrations is also suspected to contribute to the discrepancy commonly observed between laboratory and field measurements [Li et al., 2006]. A number of theoretical works have established conditions under which it is possible to accurately upscale pore scale reactive transport processes to the continuum scale [Kechagia et al., 2002; Battiato and Tartakovsky, 2011]. These studies suggest that transport phenomena dominated at the pore scale by reactive and/or advective processes require the microscopic and macroscopic scales to be considered simultaneously. The growing evidence of the importance of the pore scale is reflected in the increasing interest in modeling reactive transport in the subsurface at the this scale [Bekri et al., 1995; Salles et al., 1993; Kang et al., 2006; Tartakovsky et al., 2007a,b; Tartakovsky et al., 2008; X. Li et al., 2008; Flukiger and Bernard, 2009; Algive et al., 2010].

Pore scale modeling can be used to gain insight into the scale dependence of continuum macroscale parameters by first resolving physico-chemical processes that would otherwise not be modeled in an effective medium Darcy approach. Popular approaches to pore scale modeling applied to reactive geochemical systems include pore network models [e.g. Li et al., 2006, Algive et al., 2010], the lattice Boltzmann method [e.g. Kang et al., 2006; Van Leemput et al., 2007; Kang et al., 2010a,b] and particle methods [e.g.

Tartakovsky et al., 2007a,b; Tartakovsky et al., 2008]. Pore network models are efficient for large systems, but they need to approximate the pore geometry and the physics of the problem [e.g. Li et al., 2006]. Lattice Boltzmann models are also efficient and scalable for flow and transport problems, but they do not typically incorporate the wide range of geochemical reactions available in many geochemical models [e.g. Kang et al., 2006]. Particle methods such as the smoothed particle hydrodynamics are very robust, but are generally not applied to large systems [Tartakovsky et al., 2007a,b]. Hybrid pore scale-continuum scale models have also been developed to combine the rigorous microscopic description of the pore scale approach and the more modest computational requirements of the continuum scale approach [Van Leemput et al., 2007; Tartakovsky et al., 2008b, Battiato et al., 2011]. Existing reactive transport models based on conventional discretization methods have also been used to simulate pore scale processes when a solution of the flow field was not required, that is for diffusion-reaction problems [Navarre-Sitchler et al., 2009], or when a solution of the flow field was obtained with a lattice Boltzmann method [Yoon et al., 2012]. In conjunction with high performance computing, well-established numerical methods used in computational fluid dynamics (CFD), such as finite volume and finite difference methods, have also become practical for direct numerical simulation of flow and transport in the complex geometry of heterogeneous pore space [Trebotich et al., 2008]. Direct numerical simulation using these traditional CFD methods presents the additional advantage of ease of implementation using existing extensively-validated geochemical models that include the wide range of reactions relevant to subsurface systems.

In this work, we present a model to simulate subsurface flow and reactive transport at the pore scale by direct numerical simulation techniques based on advanced finite volume methods and adaptive mesh refinement, and apply it to the problem of carbonate mineral dissolution in porous media. Specifically, we have combined the high performance simulation tools and algorithms for incompressible flow and conservative transport in the software framework, Chombo [Trebotich et al., 2008], with the geochemical package, CrunchFlow [Steefel et al., 2003]. The objective is to demonstrate this computational tool for its use in evaluating reaction rates in natural sediments in combination with advanced characterization techniques [e.g. Peters, 2009; Armstrong and Ajo-Franklin, 2011]. Here, as an example application, we demonstrate the modeling approach to calculate average reaction rates in ideal and complex 2D and 3D geometries, using calcite dissolution with no solid-liquid geometry update. Dissolution of discrete calcite grains is described with rate laws determined in laboratory reactors, with rates normalized to physical surface area [Plummer et al., 1978]. Two verification examples are presented, one involving a single cylindrical pore investigated by Li et al [2008], and another involving an example in which calcite grains are packed into a capillary tube. In each case, for cross-validation, the pore scale results are compared with the results from continuum scale simulations using the general purpose reactive transport simulator CrunchFlow. In addition, upscaling of the reaction rates is carried out so as to assess the validity of the continuum approximation in more heterogeneous grain packs.

2. Model Description

The model considers flow, transport and geochemical reactions at the pore scale. The governing equations are the Navier-Stokes equations for incompressible flow and the advection-diffusion-reaction equations for scalar component concentration:

$$\frac{\partial \mathbf{u}}{\partial t} + (\mathbf{u} \cdot \nabla)\mathbf{u} + \nabla p = \nu \Delta \mathbf{u} \qquad (1)$$

$$\nabla \cdot \mathbf{u} = 0 \qquad (2)$$

$$\frac{\partial \rho c_k}{\partial t} + \nabla \cdot \rho \mathbf{u} c_k = \nabla \cdot \rho D_k \nabla c_k + \rho r_k \qquad (3)$$

where $\mathbf{u}$ is the fluid velocity, ∇p is the pressure gradient, c_k is the total concentration of component k, ρ is the fluid density, ν is the kinematic viscosity, D_k is the diffusion coefficient of component k in the fluid, and r_k is the rate contribution of mineral precipitation-dissolution reactions to component k per unit volume of fluid.

The domain boundary is assumed to consist of an inlet, an outlet and an impermeable lateral boundary. At the inlet boundary, velocity and concentrations are specified. In the simulations presented in this paper, the velocity at the inlet is imposed with a Poiseuille distribution profile and reported as the average value of this distribution. The outlet boundary is subject to constant pressure and a free exit condition for component concentrations. The lateral boundary is impermeable to flow and may be reactive or not.

The domain consists of solid grains and pore space occupied entirely by a single liquid phase. The system of equations (1)-(3) is discretized in the pore space of the domain

using a conservative finite volume method on a Cartesian grid. In this method, the equations are advanced in time using a predictor-corrector projection method [Trebotich and Colella, 2001; Bell et al., 1989; Chorin, 1968; D. Trebotich and D. T. Graves, An adaptive finite volume method for incompressible flow and transport in complex geometry, submitted to the *Journal of Computational Physics*, 2012]. Fluid-solid interfaces are represented as an embedded boundary within the cells that discretize the domain at a given resolution (Fig. 1). The resulting cut cells are discretized by a finite volume method that accounts for the partial volumes occupied by both fluid and solid, and for the interfacial area between fluid and solid. As discussed below, this fluid-solid interface provides the reactive surface area for dissolution-precipitation. Adaptive mesh refinement can be used to focus computations dynamically in areas of interest (e.g., at sharp concentration fronts or fluid-solid interfaces).

When flow is in the Stokes regime (in practice, when the Reynolds number, $\mathrm{Re} = |\mathbf{u}| L/\nu$, is less than 1), the term $(\mathbf{u}\cdot\nabla)\mathbf{u}$ in Eq. (1) is negligible and the model simply solves the time-dependent Stokes equation rather than the full Navier-Stokes equation. In our approach, the time-dependent procedure is used as a high resolution steady-state relaxation scheme [Trebotich and Graves, 2012] that can also be applied to time-evolving domain geometry [Miller and Trebotich, 2012]. However, when inertial forces are not negligible ($\mathrm{Re} \geq 1$), the full Eq. (1) must be solved. This may occur in accelerating and recirculating flow regions throughout the entire domain, due to local effects caused by very tortuous pore space geometries. Details of the algorithm and

solution method for flow and conservative transport are given in Trebotich and Graves [2012].

Equation (3) is solved using an operator splitting approach, where, for each timestep, transport and reactions are solved using a sequential non-iterative approach (SNIA) [Yeh and Tripathi, 1989; Steefel and MacQuarrie, 1996]. First, the conservative transport step advances the N_c total component concentrations, c_k, subject only to the fluid Courant–Friedrichs–Lewy (or CFL) condition, which constrains the timestep size Δt for a given spatial discretization Δx (i.e., $|\mathbf{u}|\Delta t/\Delta x < 1$). A higher-order upwinding scheme with a van Leer flux limiter is used for hyperbolic advection that minimizes numerical dispersion [Colella et al., 2006, van Leer, 1979]. At the end of the transport step, the nonlinear multicomponent reaction network is solved within each grid cell by a Newton method (Steefel and MacQuarrie, 1996). This 'point-by-point' calculation scales ideally with the conservative transport computations.

The geochemical step has been implemented using the CrunchFlow package, software for modeling multicomponent reactive flow and transport that has been applied to understand many complex (bio)geochemical systems [Giambalvo et al., 2002; Steefel et al., 2003; Knauss et al., 2005; Maher et al., 2006; Steefel, 2008]. Geochemical reactions are described using a mixed equilibrium and kinetic formulation that results in a nonlinear system of partial differential and algebraic equations that are solved for the concentrations of the subset of basis species. The N_r aqueous complexation reactions are assumed in equilibrium, with the concentrations of aqueous complexes calculated using

the law of mass action and included in the total component concentrations, c_k [e.g. Lichtner, 1985; Yeh and Tripathi, 1989; Steefel and Lasaga, 1994; Steefel and MacQuarrie, 1996]. Time integration is carried out with a fully implicit, backwards Euler step. Mineral dissolution-precipitation are described kinetically with the rate term (r_k). In this study, a single mineral reaction is considered and assumed to take place at the fluid-solid interface, where the reactive surface area is directly calculated as the area of the embedded boundary (Fig.1). Thus, the reactive surface area in the current pore scale model is not an additional input parameter, but is determined from the geometry of the domain. In contrast, in continuum scale models the reactive surface area is an upscaled parameter applied to a volume of porous medium and derived experimentally for a specific sample from values found in the literature for similar materials, or simply calibrated to field data.

Compared to a fully implicit approach, which solves the reaction network together with the conservative transport [Steefel and MacQuarrie, 1996], operator splitting greatly reduces the size of the (nonlinear) geochemical problem, making it much more efficient computationally for a given time step. The CFL-limited time step imposed by the higher-order explicit methods implemented in Chombo is typically more stringent than that required by the nonlinear reaction network, and, thus, the operator splitting approach does not impose an additional computational burden due to the step size.

The pore scale model does not presently account for the change in pore space geometry due to dissolution or precipitation, although it is consistent with the algorithm of Miller

and Trebotich [2012] for solving the Navier-Stokes equations on time-dependent domains. In the simulations presented here, it is assumed that the change in geometry is negligible for the short time scales necessary to reach steady state. This dynamic steady state is established as a balance between the rate at which an influent solution that is out of equilibrium with the mineral grains flows through the domain, and the rate at which the mineral reaction is driving the pore solution towards equilibrium with the mineral. Although the overall system behavior is driven by the flow of reactive fluid, the effects of molecular diffusion are accounted for explicitly, and this may become important within the hydrodynamic boundary layer surrounding mineral grains.

3. Model Validation and Demonstration

3.1. Calcite dissolution in a single cylindrical pore

To validate the pore scale model, we use the microfluidic reactive flow experiment carried out by L. Li et al. [2008] for flow through a 500 μm diameter and 4000 μm long cylindrical pore drilled in a single crystal of calcite. Input solutions of 10 mM NaCl in equilibrium with atmospheric CO_2 and adjusted to pH 4 and 5 were injected into the pore at two different average velocities within the pore of 0.04 and 0.08 cm/s. These velocities corresponded to volumetric flow rates of 4.72 and 9.39 μL min^{-1}. L. Li et al. [2008] found that using the physical area of the cylinder as reactive area and applying the model of calcite dissolution proposed by Plummer et al. [1978] and Chou et al. [1989] at the

mineral–water interface was sufficient to reproduce experiment measurements with their single-pore Poiseuille flow model. According to this model, calcite dissolution occurs via three parallel pathways:

k_1: $CaCO_3(s) + H^+ \rightarrow Ca^{2+} + HCO_3^-$ (4)

k_2: $CaCO_3(s) + H_2CO_3^* \rightarrow Ca^{2+} + 2HCO_3^-$ (5)

k_3: $CaCO_3(s) \rightarrow Ca^{2+} + CO_3^{2-}$ (6)

The rate of calcite dissolution is described by the transition state theory as the product of a far-from-equilibrium term and an affinity (or ΔG) term that goes to zero at equilibrium

$$r'_{Calcite}[mol\ m^{-2}\text{mineral}\ s^{-1}] = \left(k_1 a_{H^+} + k_2 a_{H_2CO_3^*} + k_3\right)\left(1 - \frac{a_{Ca^{2+}} a_{CO_3^{2-}}}{K_{eq}}\right) \quad (7)$$

where k_1, k_2 and k_3 are the rate constants [mol m^{-2} mineral s^{-1}]; K_{eq} is the equilibrium constant of the reaction; and a_{H^+}, $a_{H_2CO_3^*}$, $a_{CO_3^{2-}}$, and $a_{Ca^{2+}}$ are the activities of H^+, $H_2CO_3^*$, CO_3^{2-}, and Ca^{2+} [dimensionless] respectively. At 25ºC, $k_1 = 0.89$, $k_2 = 5.01\times10^{-4}$, $k_3 = 6.6\times10^{-7}$ mol m^{-2} s^{-1} [Chou et al., 1989], and log $K_{eq} = -8.234$ [Wolery et al., 1990].

We have explicitly expressed the rate of calcite dissolution in Eq. (7) as normalized to the mineral reactive surface to describe our approach for linking the physical and geochemical components of the model. Mathematically, the boundary condition for mass balance of aqueous component *k* at the mineral-solution interface can be described by

$$-D\nabla c_k \cdot \mathbf{n} = \psi\, r_k' \qquad (8)$$

where **n** is a unit vector normal to the interface, and ψ is a factor that accounts for the reactivity of a given mineral-fluid interface [m^2 reactive surface m^{-2} physical surface]. For a surface with a heterogeneous mineralogy, ψ represents the portion of surface with mineral reactions that affect the mass of component *k*, but ψ can also be used to represent enhanced reactivity due to surface roughness not resolved at this scale (i.e. ψ can be larger than 1). Experimentally, the reactive surface area of mineral is estimated from adsorption isotherms and is typically normalized to the mass [m^2 g^{-1} mineral] or volume of the bulk mineral sample [m^2 m^{-3} bulk]. In porous media at the continuum scale, the product of the reactive surface area [m^2 m^{-3} bulk] by the mineral rate r_i' [mol m^{-2} mineral s^{-1}] yields a volumetric rate. Here we take a similar approach at the pore scale in that the mineral reaction in Eq. (3) is expressed as a volumetric rate rather than as a boundary condition (Eq. 8). Assuming that $\psi = 1$, we calculate the reactive surface area at the embedded boundary cells normalized to the cell volume ($\beta dS/dV$ in Fig.1). In all other cells, the reaction rate is zero. At the fine resolutions employed in the model, where the grid block size is much smaller than the average grain size and the diffusive length scale, the boundary condition (Eq. 8) is satisfied. To recast the rate in terms of moles per unit volume as in Eq. (3), the rate expression in Eq. (7) is multiplied by the reactive surface area (physical surface area if $\psi = 1$) in units of m^2 mineral per m^3.

As discussed by L. Li et al. [2008], the average dissolution reaction rate normalized to the cylinder surface area in the pore depends on the flow rate. Experimentally, this rate, in units of mol m^{-2} s^{-1}, is obtained by mass balance between effluent and influent measured concentrations for a component involved in the dissolution reaction:

$$r'_{avg} = \frac{\left(c_k^{in} - c_k^{out}\right) Q^{tot}}{\xi_{ik} A^{tot}} \tag{9}$$

where c_k^{out}, and c_k^{in} are the effluent and influent component concentrations, respectively; Q^{tot} is the volumetric flow rate; ξ_{ik} is the stoichiometric coefficient of component *k* in the dissolution reaction *i*; and A^{tot} is the total reactive surface area (e.g. $A^{tot} = 2\pi RL$ for a cylinder of radius *R* and length *L*).

The effluent concentration is computed as a flux-weighted average at the outlet (∂S^{out})

$$c_k^{out} = \frac{\int_{\partial S^{out}} c_k \, \mathbf{u} \cdot d\mathbf{S}}{Q^{tot}} \tag{10}$$

while the volumetric flow rate can be calculated as the integration of the flux rate over the cross-sectional area, e.g. at the outlet:

$$Q^{tot} = \int_{\partial S^{out}} \mathbf{u} \cdot d\mathbf{S} \tag{11}$$

Equation (10) is used to compute and compare the concentrations measured experimentally and calculated with the current modeling approach.

We perform simulations with the same geochemical system, calcite dissolution pathways (Eq. 4-6), and rate expression (Eq. 7) of L. Li et al. [2008]. The influent solution is far from equilibrium with respect to calcite and drives dissolution of the mineral in the walls of the cylinder. As it does so, the concentration of calcium in the effluent increases. Results show that the model reproduces experimental concentrations appropriately for the experiment with an influent solution at pH 5, and also compares well with model results by L. Li et al. [2008] obtained employing the discretized Poiseuille flow solution (Fig. 2). At pH 4, the influent solution is farther from equilibrium than at pH 5 and effluent calcium concentrations are more elevated. At this pH, however, the agreement between the pore scale calculation presented here and the Poiseuille flow results and experimental data presented in Li et al (2008) is poorer. At pH 4, the concentration of H^+ is large enough that electrochemical migration leads to significant deviations from a purely Fickian treatment of diffusion [Steefel and Maher, 2009]. The pore scale model presented here does not consider the electrochemical migration term included in the global implicit implementation of CrunchFlow [Giambalvo et al., 2002] and employed by L. Li et al. [2008]. To obtain a good fit to experimental results at pH 4, the single diffusion coefficient was adjusted to an average of the diffusion of the individual species. As discussed in L. Li et al. [2008], this result indicates that mixing in the pore is incomplete and diffusion controls the degree of homogenization of the concentration field. All

additional simulations presented in this manuscript are performed at pH 5 or higher where the single diffusion coefficient Fick's law does not lead to significant errors.

In the remainder of this manuscript, we will use Eq. (9-11) to calculate average reaction rates in ideal and complex 2D and 3D geometries to illustrate the feedback between flow and reaction rates. For convenience, we will also use the same geochemical system and rate expressions.

3.2. Calcite dissolution and precipitation in a packed capillary tube

Beyond single pore systems (e.g., the experiment and model discussed in the previous section and described in Li et al, 2008), the model presented here is capable of resolving flow, multicomponent transport and reactions in porous media composed of mineral grains and pore space. To demonstrate this capability and validate the results against a 1D continuum scale model, we present two 3D simulations of calcite dissolution and precipitation in a 1 cm long capillary tube of 250 μm in diameter packed with 900 spheres of 40 μm in diameter. The physical interface area between spheres and pores and the outer surface of the cylinder are reactive calcite surfaces. In the pore scale simulation, the domain has been discretized using about 1.3 million grid points based on a grid size of 1280x32x32, which allows for a resolution of 7.8 μm. The porosity in the resulting packed capillary is 0.525 and the specific total reactive area (spheres plus cylinder wall) is $4.53 \cdot 10^4$ m^2 m^{-3}. These continuum scale parameters obtained from direct upscaling of the pore scale model have been directly used in an equivalent continuum scale reactive

transport simulation (Table 1). This simulation has been performed with CrunchFlow on a 1D domain discretized with 160 cells. Both pore scale and continuum scale models use the exact same subroutines to calculate the multicomponent reaction network. In the dissolution simulation, the inlet solution of section 3.1 at pH 5 flows from left to right with a velocity at the inlet of 0.035 cm s^{-1}, dissolving calcite making up the solid grains according to Eq. (4)-(7). In the precipitation simulation, a solution at pH 8.48, supersaturated with respect to calcite (1 mM $CaCl_2$, 2 mM $NaHCO_3^-$, in equilibrium with atmospheric CO_2), flows from left to right at a velocity at the inlet of $6.7 \cdot 10^{-4}$ cm s^{-1}. It is assumed that nucleation of calcite for precipitation occurs uniformly on the solid grain surface. The rate expression in Eq. (7) is simplified to include only the zero order term (i.e. $k_1 = k_2 = 0$) with $k_3 = 1.58 \cdot 10^{-9}$ mol m^{-2} s^{-1} (C. Noiriel et al., Upscaling calcium carbonate precipitation rates from core to continuum scale, submitted to *Chemical Geology*, 2012) for a single precipitation pathway:

$$Ca^{2+} + CO_3^{2-} \rightarrow CaCO_3(s) \qquad (12)$$

Concentration results from the pore scale and continuum scale simulations are shown in Fig. 3. The overlapping calcium concentration profiles indicate that the capillary tube with its large aspect ratio behaves effectively as a one dimensional system. While the specific reactive surface area in the pore scale model is directly the area corresponding to the interface between the calcite grains and the pore space, in the continuum model the reactive surface area is a continuum scale value that applies to each cell of the domain. Using the value scaled-up from the pore scale to the continuum model gives a good

match between both models in this simulation due to the one dimensional behavior of the system. There is a slight disagreement between models (pore scale and continuum) near the inlet and near the outlet due to a small offset in the packing of the spheres from the boundaries that is reflected in the change of slope in the pore scale model results.

3.3. Calcite dissolution in a large 3D domain

To understand the effects of complex flow patterns on reaction rates in natural sediments, a pore scale model needs to be able to perform efficient computations on large domains discretized at fine resolution. Current synchrotron based x-ray computed microtomography techniques are capable of capturing high resolution images of porous media. For example, Armstrong and Ajo-Franklin [2011] resolved the pore scale at a 4.5 μm resolution of a 12 mm long and 8 mm diameter experimental column of carbonate precipitation imaged at the Advanced Light Source at Lawrence Berkeley National Laboratory. The simulation presented in section 3.2 of dissolution in a capillary tube has been performed at the comparable resolution of 7.8 μm. Here, we demonstrate our modeling approach for high performance computations on larger pore space domains. We perform a simulation of a 1 cm long, 0.5 cm in diameter cylinder randomly packed with 1200 spheres with 250 μm radius each, resulting in 60% porosity (Fig. 4). The same geochemical problem as in the previous examples is considered, with calcite dissolving as a solution at pH 5 is injected at the inlet at a rate of 0.04 cm s^{-1}. The domain was discretized with approximately 33.5 million grid points based on a regular grid of 512x256x256 for a grid block resolution of 19.5 μm (Table 1). The simulation was run on

NERSC supercomputers (Cray XT4 and Cray XE6), using 1024 cores and averaging 0.6 GB of memory per core. A total transport step consumed 17.12 seconds of wall clock time with 90% of the time spent in conservative transport and slightly less than 10% in geochemical reaction calculations. Each total transport step takes approximately a third of the time of a velocity step in the steady-state incompressible flow computation. These results show that the requirements for solving the incompressible flow field are greater than those for solving transport field, and these in turn greater than those for the geochemical step, thus, validating our operator splitting approach.

4. Dependence of average dissolution rates on pore scale flow in ideal 2D geometries

To illustrate the scaling effects as a result of flow heterogeneity at the pore scale, three 2-dimensional 1-cm long 0.5-cm wide domains packed with 378 cylindrical grains were generated. In one, the grains are uniformly distributed as a staggered array (Fig. 5); in a second, calcite grains are randomly packed so as to produce a more heterogeneous medium at the pore scale (Fig. 5); and in a third, calcite grains are packed randomly in two distinct zones, the upper half and lower half with tighter and looser packing, respectively (Fig. 5). The resulting packing in the third domain is heterogeneous at the pore scale, but also at a scale that encompasses several pores. The grains represent calcite that dissolves as the solution undersaturated with respect to calcite (pH 5) flows left-to-right through the domain (section 3). The three domains have equivalent average geochemical parameters: the cylinder radii are 100 μm, resulting in a porosity of 0.76 porosity, and calcite specific surface area for the domain of 4750 m^2 m^{-3} (Table 1).

As in Section 3.2, we have run 1D continuum scale reactive transport simulations with CrunchFlow for comparison using the pore-scale-derived continuum-scale parameters (Table 1). These simulations were run to steady state for a range of velocities, and the averaged area-normalized dissolution reaction rate was calculated according to Eq. (9) for all of them (Fig. 6). For slow velocities (up to 0.001 cm s^{-1}), the average rate is limited by the transport rate as the reaction rate is fast enough to keep the system close to equilibrium. For fast velocities (> 10 cm s^{-1}), the average rate is limited by the intrinsic kinetic reaction rate, that is, the rate is surface reaction-controlled. In this example, this rate is mostly attributable to the dissolution pathway of Eq. (4), described as a function of a_{H^+} in Eq. (7), because the influent solution has pH 5. As a result, at both ends of the velocity spectrum, pore scale effects are likely to be negligible and the system behaves like a 1D domain. For intermediate velocities, the average rate will depend on the two-dimensional interplay between flow and reaction that takes place at the pore scale. Here we choose to run the simulations with an inlet velocity of 0.1 cm s^{-1} that falls within the range of intermediate velocities, but is an upper bound of velocities encountered under natural conditions. This reflects the fact that calcite dissolution is a relatively fast reaction that is typically in equilibrium (transport limited) under natural conditions. For intermediate velocities for this domain, the change in curvature of the curve (Fig. 6) reflects the kinetic limitation expressed by the rate constant k_3 (Eq. 6) included in the calcite dissolution model employed.

While the simulations share the same average geochemical parameters, the different configurations give rise to differences in the flow patterns at the pore scale (Fig. 5, left panels), which in turn affect the steady state effluent concentrations and thus the average dissolution reaction rates (7.79×10^{-11} mol cm^{-2} s^{-1} for the regular configuration, 7.24×10^{-11} mol cm^{-2} s^{-1} for the one-zone heterogeneous configuration, and 6.88×10^{-11} mol cm^{-2} s^{-1} for the two-zone heterogeneous configuration). Visually, the resulting concentration fronts produced in the pore scale simulations at steady state are also different (Fig. 5, right panels). While the regular configuration behaves like a 1D system, in spite of boundary effects, the fronts in the heterogeneous configurations show irregular patterns. In the one-zone heterogeneous configuration, a 2D flame-like pattern develops in which concentration gradients are visible inside individual pores. Some flow paths where flow is slower (dark blue in the left panel) leave some pores with higher concentrations of total calcium (dark red in the right panel) and fast flow paths (red in left panel) with concentrations closer to influent conditions (dark blue). Due to this heterogeneity in flow pattern, for a given flow rate, average rates for the regular (homogeneous) configuration are larger than for the heterogeneous configuration. The effect of heterogeneity is more exaggerated in the two-zone heterogeneous configuration. Flow is much faster in the lower half of the domain as shown in Fig 5 (left panel), and the solution is closer to influent conditions (dark blue). The faster velocities move the conditions in the lower half of the domain to the right along the x-axis of Fig. 6, toward surface reaction-limiting conditions. On the other hand, the upper half of the domain has slow velocities that allow the solution to equilibrate with the calcite in the grains (the equilibrium total calcium concentration is 2.6×10^{-7} mol cm^{-3}) moving the system to the left along the x-axis of Fig.

6, toward transport limiting conditions. When the solution comes to equilibrium with calcite along a particular flow path, the calcite grains down-gradient do not dissolve. Although the reactive area of these grains is available and accounted for in the averaging calculations, e.g. in Eq. (9), the grains do not react. As a result, the average reaction rate is lower than in the regular and one-zone heterogeneous domains. The average reaction rate calculated in the 1D continuum simulation (8.62×10^{-11} mol cm^{-2} s^{-1}) is larger than any of the pore scale simulation results, since 1D flow is uniform, and therefore the model does not account for regions of the domain that do not contribute to calcite dissolution.

5. Discussion

From the simulations presented above, it is apparent that average reaction rates depend on the flow pattern within porous media and the concentration gradients that develop at the pore scale. If one thinks of the 1-cm-long 0.5-cm-wide simulation domains as individual discretization cells of a larger continuum scale model to which single parameter values are assigned, the question arises as to how to upscale the reactive parameters (i.e., surface area, rate constants) to capture the pore scale information. Here, the three domains were generated with equivalent reactive surface areas (and porosity), and the same rate constants from the literature were used and applied at the pore scale, and yet different average rates were obtained. In a continuum scale simulation, for the same flow rate and incoming concentrations, and using equivalent reactive parameters, computations would

produce the exact same rates in the three cells. The pore scale information would be lost in such simulations.

In the process of upscaling solute transport, microscale information is reduced by using a set of scaling laws [Wood, 2009, 2010]. Such scaling laws represent statements on the structure of microscale processes and impose conditions on the upscaling process. Theoretical works have established the conditions under which upscaling techniques provide accurate descriptions of pore-scale processes [Kechagia et al., 2002; Battiato and Tartakovsky, 2011]. Although these studies have focused on single component systems and kinetic formulations, which are more amenable to analytical manipulations, it is illustrative nevertheless to attempt here to compare simulation results from this work with these theoretical results. In particular, we seek to locate where on the phase diagram of Battiato and Tartakovsky [2011] the simulations presented here would fall. This diagram shows the range of applicability of the macroscopic equations as a function of the Peclet number ($Pe = UL/D$) and the diffusive Damköhler number ($Da = r''L/D$). In multicomponent systems subject to aqueous speciation, the calculation of the Damköhler number is not straightforward. Here we simply normalize the overall kinetic limited rate noted as a horizontal line in Fig. 6 (r' [mol cm^{-2} s^{-1}]), by the concentration of calcium at equilibrium with calcite, i.e. $r'' = r'/c_{Ca}^{eq}$. Based on the scale parameter, $\varepsilon = \text{grain size}/L$, the point corresponding to the 2D simulations of section 4 fall in the reaction-and-advection-dominated region of the diagram with $(-\log_{\varepsilon} Pe, \log_{\varepsilon} Da) = (1.36, -1.07)$. In this region, the macroscale and microscale are coupled. The results presented in section 4, which were obtained by direct numerical simulation of pore scale processes rather by

mathematical analysis, support this observation. . For the simulation domains, no assumption was made on the pore scale velocity and concentrations fields–they were resolved directly–and an averaging method was used to calculate a reaction rate for the domain given that reactions represent a mass balance of reactants and products within a given porous volume. Generally, such averages can be used as a measure of the magnitude of the deviation from the parameter values that are used in the discretized equations of the continuum scale model, but no scaling law is derived in this process.

An objective of this study is to understand the discrepancy between laboratory-determined and continuum (field scale) model rates. Here, the discrepancy in average calcite dissolution rates in domains with equivalent reactivity is attributed to the non-uniformity of flow. Our simulations demonstrate that average rates obtained from the model simulations decrease with increasing heterogeneity of the grain pack. This result is in agreement with the observation that dissolution rates of many minerals have been found to be slower in the field than those measured in the laboratory. However, the small differences obtained in the simulations cannot explain the orders of magnitude difference between field and lab experiments, although larger scale and hierarchical heterogeneity structures could magnify this effect significantly [Malmstrom et al, 2000]. Once an update of the pore space geometry based on the algorithm of Miller and Trebotich [2012] for moving boundaries is implemented, it will be possible to consider the additional effect of increasing heterogeneity as a result of geochemical reactions. Based on the dynamics, we expect this effect to be largest in the case of dissolution, since “wormholing” may

develop, resulting in strongly preferential flow paths [Hoefner and Fogler, 1988; Steefel and Lasaga, 1990; Steefel and Maher, 2009].

Additionally, we have focused this study on calcite dissolution because it is a relevant reaction in many environments, but it is also a relatively fast reaction with the pore water typically reaching thermodynamic equilibrium with respect to calcite at relatively small spatial scales. Even though microscale and macroscale are still coupled in these conditions [Kechagia et al., 2002], as shown by the simulation results above, the effect of pore scale flow on reaction rates may be larger for reactions with slow kinetics.

The simplified textural and mineralogical systems considered in this work have been used to demonstrate the modeling approach. This development, however, is intended to be more general in that the model presented here can incorporate the physical and geochemical heterogeneity of natural sediments obtained as characterized using the advanced microscopic techniques that are becoming available [e.g. Armstrong and Ajo-Franklin, 2011; Peters, 2009]. Ultimately the objective is to simulate reactive transport at the pore scale using a computationally efficient platform in order to provide estimates of realistic reaction rates in natural sediments. This approach can be used to inform continuum scale models, and at the same time to mechanistically understand the processes that lead to rate discrepancies in field applications. Such knowledge is necessary to improve the predictive capability of field scale models.

Acknowledgements

The authors would like to thank Gunther Weber (Lawrence Berkeley National Laboratory) for his support in the post-processing and visualization of simulation results, and Li Li (Penn State) for providing the input and source files to reproduce the original results of section 3.1. This material is based upon work supported as part of the Center for Nanoscale Control of Geologic CO_2, an Energy Frontier Research Center funded by the U.S. Department of Energy, Office of Science, Office of Basic Energy Sciences, and the Office of Advanced Scientific Computing SciDAC program, under Award Number DE-AC02-05CH11231. This research used resources of the National Energy Research Scientific Computing Center, which is supported by the Office of Science of the U.S. Department of Energy under Contract No. DE-AC02-05CH11231.

References

Algive, L., Bekri, S., and Vizika, O. (2010), Pore-Network Modeling Dedicated to the Determination of the Petrophysical-Property Changes in the Presence of Reactive Fluid. *SPE J.* **15** (3): 618-633. SPE-124305-PA. doi: 10.2118/124305-PA.

Armstrong, R., and J Ajo-Franklin (2011), Investigating biomineralization using synchrotron based X-ray computed microtomography, *Geophys. Res. Lett*., 38, L08406, doi:10.1029/2011GL046916, 2011

Bain, J.G., K. U. Mayer, D. W. Blowes, E. O. Frind, J. W. H. Molson, R. Kahnt, U. Jenk (2001), Modelling the closure-related geochemical evolution of groundwater at a former uranium mine, *J. Contam. Hydrol*., 52(1-4), 109 – 135.

Battiato, I., and D.M. Tartakovsky (2011) Applicability regimes for macroscopic models of reactive transport in porous media, *J. Contam. Hydrol.* 120–121, 18–26.

Battiato, I., D.M. Tartakovsky, A.M. Tartakovsky, and T.D. Scheibe (2011), Hybrid models of reactive transport in porous and fractured media, *Adv. Water Resour.* ,34(9): 1140 – 1150.

Bell, J. B., P. Colella, and H. M. Glaz (1989). A second-order projection method for the incompressible Navier-Stokes equations. *J. Comput. Phys.*, 85:257-283.

Bekri, S., J. F. Thovert, and P. M. Adler (1995), Dissolution of porous media, *Chem. Eng. Sci.*, 50, 2765– 2791.

Bruant, R. G., A. J. Guswa, M. A. Celia, and C. A. Peters (2002). Safe storage of CO2 in deep saline aquifers. Environmental Science & Technology, 36(11):240A-245A.

Chorin, A. J. (1968), Numerical solutions of the Navier-Stokes equations. *Math. Comp*., 22:745-762.

Chou, L., Garrels R. M. and Wollast R. (1989) Comparative study of the kinetics and mechanisms of dissolution of carbonate minerals. *Chem. Geol*. 78, 269–282.

Colella, P., D.T. Graves, B.J. Keen, and D. Modiano (2006), A Cartesian grid embedded boundary method for hyperbolic conservation laws. *J. Comp. Phys.* 211, 347-366.

Essaid, H.I., I.M. Cozzarelli, R.P. Eganhouse, W.N. Herkelrath, B.A. Bekins, and G.N. Delin, G.N. (2003), Inverse modeling of BTEX dissolution and biodegradation at the Bemidji, MN crude-oil spill site. *J. Contam. Hydrol*., 67(1-4), 269-299, doi:10.1016/S0169-7722(03)00034-2.

Flukiger, F. , D. Bernard (2009), A new numerical model for pore scale dissolution of calcite due to CO2 saturated water flow in 3D realistic geometry: Principles and first results, *Chem. Geol.*, 265 (2009) 171–180

Giambalvo E. R., Steefel C. I., Fisher A. T., Rosenberg N. D. and Wheat C. G. (2002) Effect of fluid-sediment reaction on hydrothermal fluxes of major elements, eastern flank of the Juan de Fuca Ridge. *Geochim. Cosmochim. Acta* 66(10), 1739–1757.

Hoefner, M. L. and H.S. Fogler (1988), Pore evolution and channel formation during flow and reaction in porous media, *Am. Inst. Chem. Engin. J.*, 34, 45-54.

Kang, Q., P. C. Lichtner, and D. Zhang (2006), Lattice Boltzmann pore-scale model for multicomponent reactive transport in porous media, *J. Geophys. Res.*, 111, B05203, doi:10.1029/2005JB003951.

Kang, Q., P.C. Lichtner, and D.R. Janecky (2010), Lattice Boltzmann Method for Reacting Flows in Porous Media, *Adv. Appl. Math. Mech.*, 2(5), 545-563.

Kang, Q., P.C. Lichtner, H.S. Viswanathan, A.I. Abdel-Fattah (2010), Pore Scale Modeling of Reactive Transport Involved in Geologic CO_2 Sequestration, *Transp. Porous Med.* , 82:197–213

Kechagia, P. E., I. N. Tsimpanogiannis, Y. C. Yortsos, and P. Lichtner (2002), On the upscaling of reaction-transport processes in porous media with fast or finite kinetics, *Chem. Eng. Sci.*, 57, 2565– 2577.

Knauss K. G., J.W. Johnson, and C.I. Steefel (2005) Evaluation of the impact of CO_2, co-contaminant gas, aqueous fluid and reservoir rock interactions on the geologic sequestration of CO_2. *Chem. Geol.* 217, 339–350.

Van Leemput, P. , C. Vandekerckhove, W. Vanroose, and D. Roose (2007), Accuracy of hybrid lattice Boltzmann/finite difference schemes for reaction-diffusion systems, *SIAM J. Multiscale Model. Simul.*, 6: 838–857.

Van Leer, B. (1979), Towards the ultimate conservative difference scheme, V: A second-order sequel to Godunov's method. *J. Comput. Phys.* 32, 101–136.

Li, L., C. A. Peters, and M. A. Celia (2006), Upscaling geochemical reaction rates using pore-scale network modeling. *Adv. Water Resour.*, 29(9):1351-1370.

Li, L., C. I. Steefel, and L. Yang (2008), Scale dependence of mineral dissolution rates within single pores and fractures. *Geochim. Cosmochim. Acta*, 72(2):360-377.

Li, L., C. I. Steefel, K. H. Williams, M. J. Wilkins, and S. S. Hubbard (2009), Mineral Transformation and Biomass Accumulation Associated With Uranium Bioremediation at Rifle, Colorado, *Environ. Sci. Technol.*, 43 (14), 5429–5435, doi:10.1021/es900016v.

Li, X., H. Huang, and P. Meakin (2008), Level set simulation of coupled advection-diffusion and pore structure evolution due to mineral precipitation in porous media, *Water Resour. Res.*, 44, W12407, doi:10.1029/2007WR006742, 2008

Lichtner, P. (1985), Continuum model for simultaneous chemical- reactions and mass-transport in hydrothermal systems, *Geochim. Cosmochim. Acta*, 49 (3), 779–800, doi:10.1016/0016-7037(85)90172-3.

Malmström, M.E., G. Destouni, S.A. Banwart, and B.H. E. Strömberg (2000), Resolving the scale-dependence of mineral weathering rates, *Environ. Sci. Technol.* 34 (7), 1375-1378

Maher K., C.I. Steefel, D.J. DePaolo and B.E. Viani (2006), The mineral dissolution rate conundrum: insights from reactive transport modeling of U isotopes and pore fluid chemistry in marine sediments. *Geochim. Cosmochim. Acta* 70(2), 337–363.

Maher, K., C. I. Steefel, A. F. White, and D. A. Stonestrom (2009), The role of reaction affinity and secondary minerals in regulating chemical weathering rates at the Santa Cruz

Soil Chronosequence, California, *Geochim. Cosmochim. Acta*, 73 (10), 2804–2831, doi:10.1016/j.gca.2009.01.030.

Miller, G. H. and D. Trebotich (2012), An embedded boundary method for the Navier-Stokes equations on a time-dependent domain, *Commun. Appl. Math Comp. Sci.,* 7(1):1-31.

Molins, S., K.U. Mayer, R.T. Amos, and B.A. Bekins (2010),Vadose zone attenuation of organic compounds at a crude oil spill site - Interactions between biogeochemical reactions and multicomponent gas transport, *J. Contam. Hydrol,* 112(1-4), 15-29.

Navarre-Sitchler, A., C.I. Steefel, L. Yang, L. Tomutsa, and S.L. Brantley (2009), Evolution of porosity and diffusivity associated with chemical weathering of a basalt clast, *J. Geophys. Res.*, 114, F02016, doi:10.1029/2008JF001060.

Noiriel C., L. Yang, J.B. Ajo-Franklin. and C.I. Steefel (2011), Upscaling calcium carbonate precipitation rates from pore to continuum scale, *Chem. Geol., submitted.*

Pacala, S., and R. Socolow (2004). Stabilization wedges: Solving the climate problem for the next 50 years with current technologies. *Science*, 305(5686):968-972.

Peters, C. A. (2009), Accessibilities of reactive minerals in consolidated sedimentary rock: An imaging study of three sandstones, *Chem. Geol.*, 265 (1-2), 198–208, doi:10.1016/j.chemgeo.2008.11.014

Plummer, L. N., Wigley T. M. L. and Parkhurst D. L. (1978) The kinetics of calcite dissolution in CO2–water systems at 5 degree C to 60 degree C and 0.0 to 1.0 atm CO_2. Am. J. Sci. 278, 179–216.

Prommer, H., N. Tuxen, and, P.L. Bjerg (2006), Fringe-Controlled Natural Attenuation of Phenoxy Acids in a Landfill Plume: Integration of Field-Scale Processes by Reactive Transport Modeling, *Environ. Sci. Technol.* 40 (15), 4732-4738.

Salles, J., J. F. Thovert, and P. M. Adler (1993), Deposition in porous media and clogging, *Chem. Eng. Sci.*, 48, 2839–2858.

Steefel, C. I. (2008) CrunchFlow User's Manual. Lawrence Berkeley National Laboratory, Berkeley, Cal.

Steefel, C.I. and A.C. Lasaga (1990), The evolution of dissolution patterns: Permeability change due to coupled flow and reaction. In *Chemical Modeling of Aqueous Systems II* (eds. D. Melchior and R.L. Bassett), ACS Symposium Series No. 416, American Chemical Society, Washington, 212-225.

Steefel C. I. and Lasaga A. C. (1994) A coupled model for transport of Hydrothermal fluxes of major elements, Juan de Fuca flank 1755 multiple chemical species and kinetic precipitation/dissolution reactions with application to reactive flow in single phase hydrothermal systems. *Am. J. Sci.* 294, 529–592.

Steefel, C.I., and K. MacQuarrie (1996), Approaches to modeling of reactive transport in porous media, *in Reactive Transport In Porous Media, Reviews in Mineralogy*, vol. 34, edited by Lichtner, PC and Steefel, CI and Oelkers, EH, pp. 83–129, Mineral Soc Amer., Washington, DC.

Steefel C. I., Carroll S., Zhao P. and Roberts S. (2003) Cesium migration in Hanford sediment: a multisite cation exchange model based on laboratory transport experiments. *J. Contam. Hydrol.* 67(1-4), 219–246.

Steefel, C. I., D. J. DePaolo, and P. C. Lichtner (2005), Reactive transport modeling: An essential tool and a new research approach for the Earth sciences. *Earth Planet. Sci. Lett.*, 240(3-4):539-558.

Steefel, C.I., and K. Maher (2009), Fluid-rock interaction: A reactive transport approach *in Reviews in Mineralogy and Geochemistry, vol. 70, pp. 485-532*, Min. Soc. Am., Washington, D.C., doi 10.2138/rmg.2009.70.11.

Tartakovsky, A.M., P. Meakin, T. D. Scheibe, and R. M. E. West (2007). Simulations of reactive transport and precipitation with smoothed particle hydrodynamics. *J. Comp. Phys.*, 222:654–672.

Tartakovsky, A. M., P. Meakin, T. D. Scheibe, and B. D. Wood (2007), A smoothed particle hydrodynamics model for reactive transport and mineral precipitation in porous and fractured porous media, *Water Resour. Res.*, 43, W05437, doi:10.1029/2005WR004770.

Tartakovsky, A. M., G. Redden, P. C. Lichtner, T. D. Scheibe, and P. Meakin (2008a), Mixing-induced precipitation: Experimental study and multiscale numerical analysis, *Water Resour. Res.*, 44, W06S04, doi:10.1029/2006WR005725.

Tartakovsky, A. M., D. M. Tartakovsky, T. D. Scheibe, and P. Meakin (2008b), Hybrid Simulations of Reaction-Diffusion Systems in Porous Media, *SIAM J. Sci. Comput.*, 30(6): 2799-2816.

Trebotich, D, and P. Colella (2001), A projection method for incompressible viscous flow on a deformable domain. *J. Comput. Phys*., 166, 191-217.

Trebotich, D., B. Van Straalen, D. T. Graves, and P. Colella (2008), Performance of embedded boundary methods for CFD with complex geometry. *J. Phys. Conf. Ser.*, 125:012083.

Trebotich, D, and D. T. Graves (2012), An adaptive finite volume method for incompressible flow and transport in complex geometry. *J. Comput. Phys*. under review

Thullner, M., P. Van Cappellen, and P. Regnier (2005), Modeling the impact of microbial activity on redox dynamics in porous media, *Geochim. Cosmochim. Acta*, 69(21),5005-5019.

Wang, S.; P.R. Jaffe, G. Li, S.W. Wang, and H.A. Rabitz (2003), Simulating bioremediation of uranium-contaminated aquifers; uncertainty assessment of model parameters. *J. Contam. Hydrol.*, 64, 283–307.

White, C. M., B. R. Strazisar, E. J. Granite, J. S. Homan, and H. W. Pennline (2003), Separation and capture of CO2 from large stationary sources and sequestration in geological formations—Coalbeds and deep saline aquifers, *J. Air Waste Manage. Assoc.*, 53(6): 645-715.

Wolery, T. J., K. J. Jackson, W. L. Bourcier, C. J. Bruton, B. E. Viani, K. G. Knauss, and J. M. Delany (1990), Current status of the EQ3/6 software package for geochemical modeling, in Chemical Modeling in Aqueous Systems II, ACS Symp. Ser. No. 416, edited by D. C. Melchior and R. L. Basset, 104–116, Am. Chem. Soc., Washington, D.C.

Wood BD. (2009), The role of scaling laws in upscaling. *Adv. Water Resour.*, 32, 723–736.

Wood BD. (2010), Reply to comment by Philippe Baveye on‘‘The role of scaling laws in upscaling. *Adv. Water Resour.*, 33, 125–127.

Yeh G. T. and Tripathi V. S. (1989), A critical evaluation of recent developments in hydrogeochemical transport models of reactive multichemical components. *Water Resour. Res.* 25, 93–108.

Yoon, H., A. J. Valocchi, C. J. Werth, and T. A. Dewers (2012) Pore-scale simulation of mixing-induced calcium carbonate precipitation and dissolution in a microfluidic pore network, *Water Resour. Res.*, doi:10.1029/2011WR011192, in press.

Zhang, D. X., R. Y. Zhang, S. Y. Chen, and V. E. Soll (2000), Pore scale study of flow in porous media: Scale dependency, REV, and statistical REV. *Geophys. Res. Lett.*, 27(8):1195-1198.

Figure Captions

Figure 1. Schematic showing a portion of a 2D regular discretization grid cut by a fluid-solid interface. A cut-cell is highlighted to illustrate the embedded boundary concept. The fluid volume of the cut-cell is a fraction α of a regular cell volume (dV), while the fluid-solid interfacial surface area is a fraction β of a maximum interfacial area (dS). Only for cut-cells is this fraction non-zero ($\beta \neq 0$), and these cells are reactive in the pore scale model.

Figure 2. Comparison of the flux-weighted average concentration of total calcium calculated from the current model with the measured concentration from the outlet of the microfluidic reactive flow experiment and Poiseuille flow model by L. Li et al. [2008] under two different pH and flow conditions. See text for discussion of the effect of neglecting electrochemical migration.

Figure 3. Comparison of total calcium concentrations in the simulation of (a) dissolution and (b) precipitation in a capillary tube packed with calcite spheres using a pore scale model (solid line) and an equivalent continuum scale model (symbols). Concentrations in the pore scale model are flux-weighted averages in each cross section. The inset shows the midplane total calcium concentration contours in a 0.25 cm-long section of the capillary tube for the dissolution simulation.

Figure 4. Calcium concentration contours for the large 3D domain. Concentrations units are mol cm^{-3}.

Figure 5. Absolute velocity magnitude (left) and total calcium concentration (right) contours for (a) regular staggered array of calcite grains, (b) one-zone heterogeneously packed calcite grains, and (c) heterogeneously packed calcite grains in two-zone domain. Velocity in cm s^{-1} and concentrations in mol cm^{-3}.

Figure 6. Steady-state calcite dissolution rates calculated using a 1D continuum model of the 2D array of calcite grains as a function of the flow velocity using a double logarithmic scale.

Tables

Table 1. Simulation parameters

Simulation (Section #)	Dimensions (Grid points)	Length (Resolution)	Porosity	Specific Reactive Area
Poiseuille flow in cylindrical pore (3.1)	512x64x64 (10 million)	0.4 cm (7.8 μm)	1.0	8000 m^2 m^{-3}
Capillary tube packed with calcite spheres (3.2)	1280x32x32 (1.3 million)	1 cm (7.8 μm)	0.525	$4.53 \cdot 10^4$ m^2 m^{-3}
Cylinder packed with calcite spheres (3.3)	512x256x256 (33.5 million)	1 cm (19.5 μm)	0.6	5600 m^2 m^{-3}
2D array of calcite grains (4)	1024x512 (0.524 million)	1 cm (9.76 μm)	0.7625	$4750 \cdot m^2$ m^{-3}

Figures

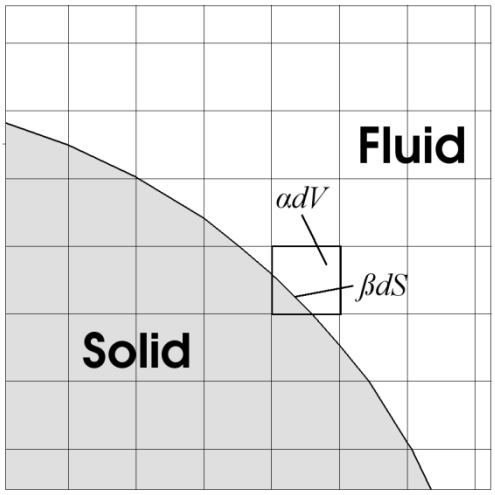

Figure 1. Schematic showing a portion of a 2D regular discretization grid cut by a fluid-solid interface. A cut-cell is highlighted to illustrate the embedded boundary concept. The fluid volume of the cut-cell is a fraction α of a regular cell volume (*dV*), while the fluid-solid interfacial surface area is a fraction β of a maximum interfacial area (*dS*). Only for cut-cells is this fraction non-zero ($\beta \neq 0$), and these cells are reactive in the pore scale model.

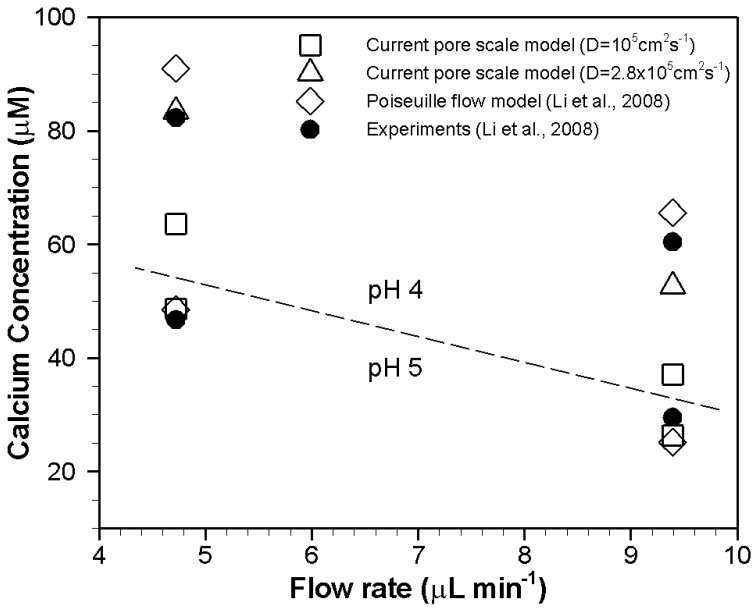

Figure 2. Comparison of the flux-weighted average concentration of total calcium calculated from the current model with the measured concentration from the outlet of the microfluidic reactive flow experiment and Poiseuille flow model by L. Li et al. [2008] under two different pH and flow conditions. See text for discussion of the effect of neglecting electrochemical migration.

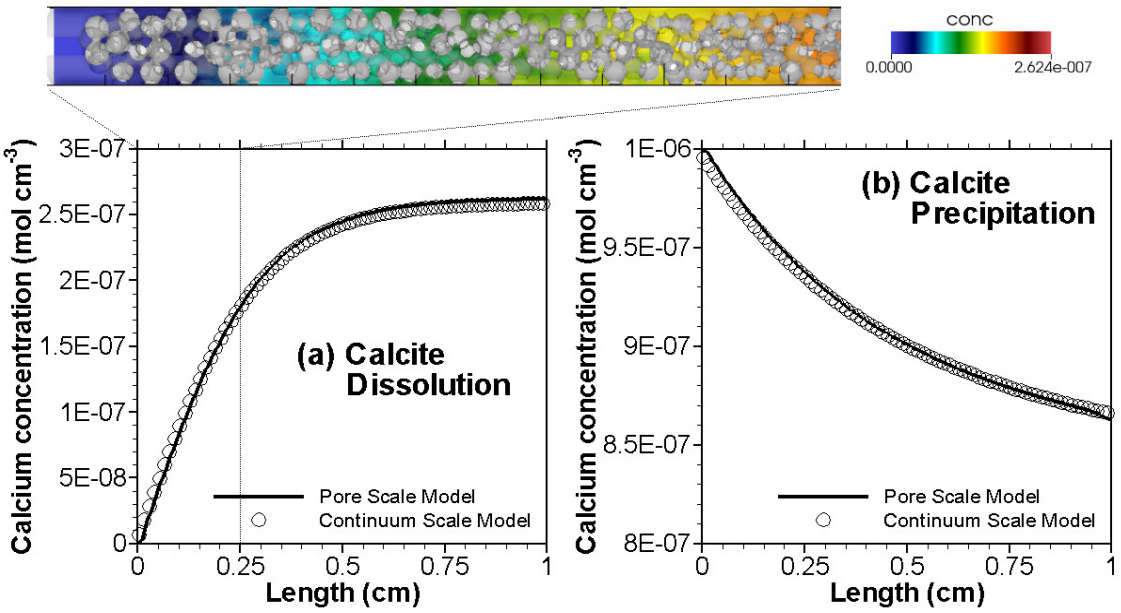

Figure 3. Comparison of total calcium concentrations in the simulation of (a) dissolution and (b) precipitation in a capillary tube packed with calcite spheres using a pore scale model (solid line) and an equivalent continuum scale model (symbols). Concentrations in the pore scale model are flux-weighted averages in each cross section. The inset shows the midplane total calcium concentration contours in a 0.25 cm-long section of the capillary tube for the dissolution simulation.

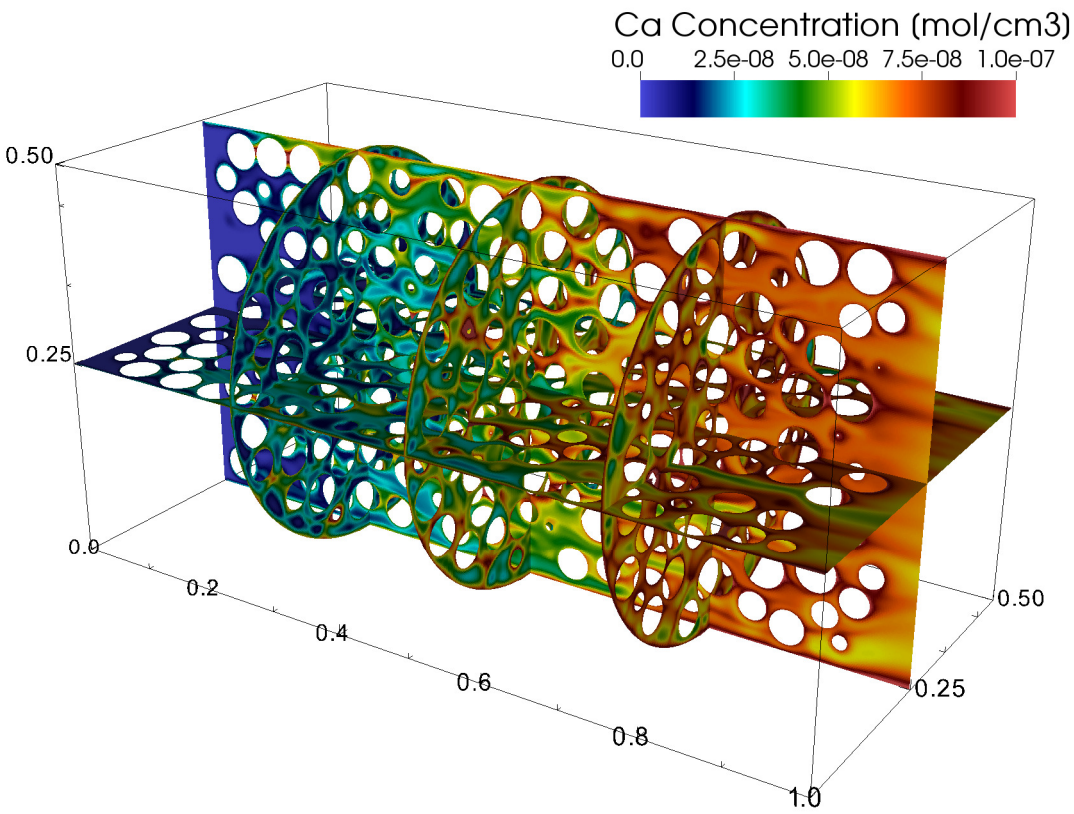

Figure 4. Calcium concentration contours for the large 3D domain. Concentrations units are mol cm^{-3}.

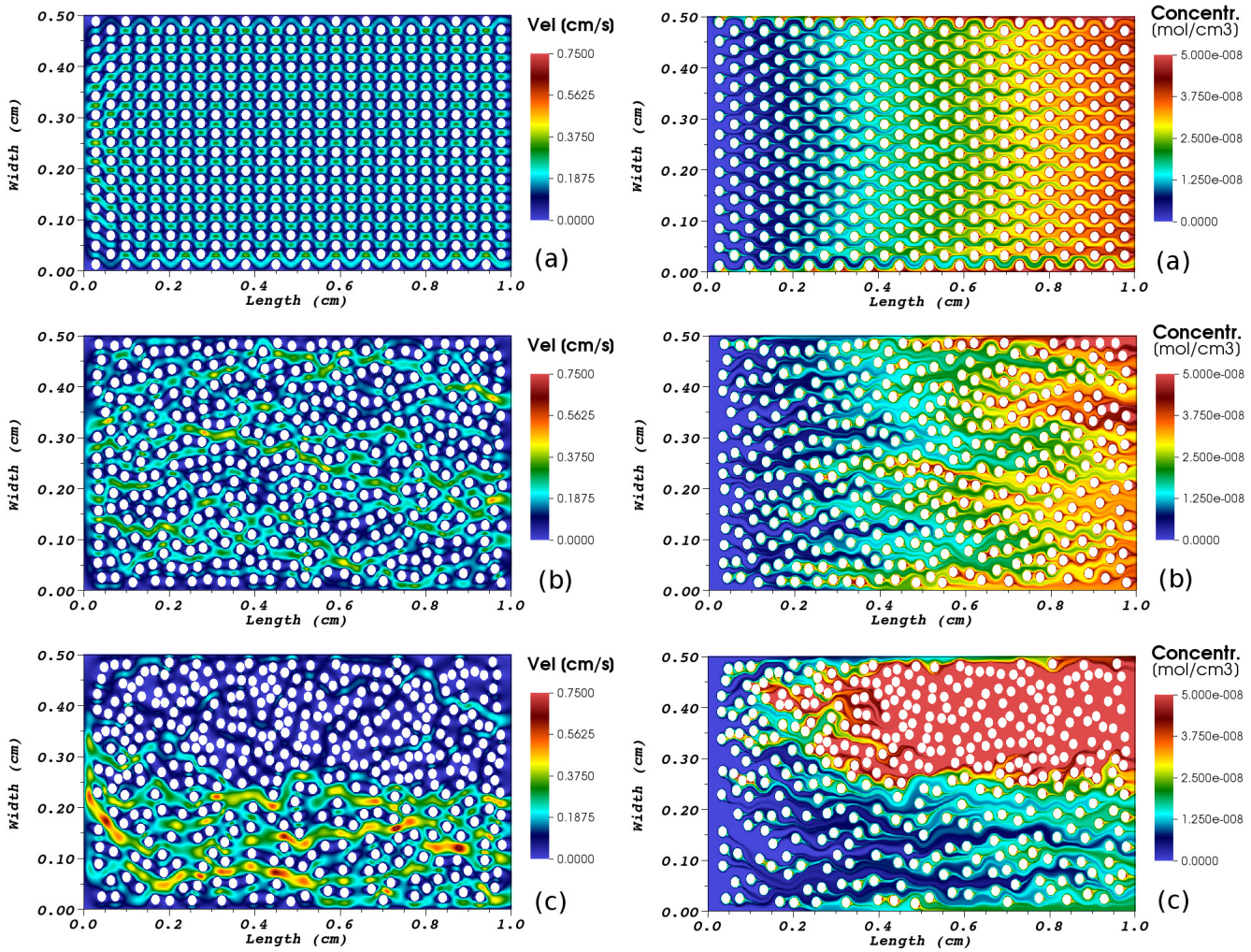

Figure 5. Absolute velocity magnitude (left) and total calcium concentration (right) contours for (a) regular staggered array of calcite grains, (b) one-zone heterogeneously packed calcite grains, and (c) two-zone heterogeneously packed calcite grains in two-zone domain. Velocity in cm s^{-1} and concentrations in mol cm^{-3}.

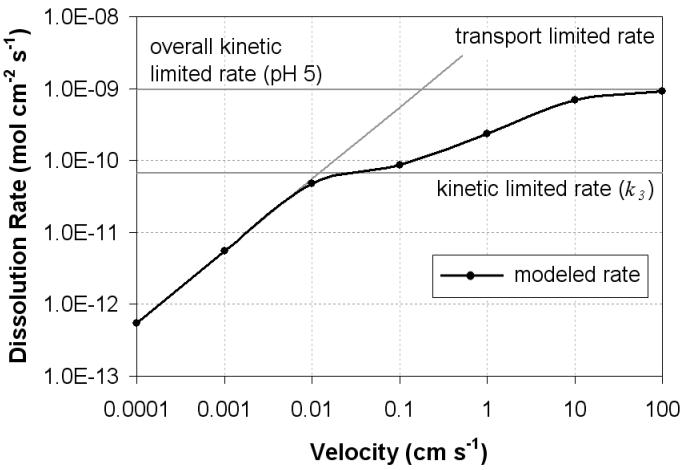

Figure 6. Steady-state calcite dissolution rates calculated using a 1D continuum model of the 2D array of calcite grains as a function of the flow velocity using a double logarithmic scale.